Plasma Sources Sci. Technol. **18** (2009) 014015 (16pp) doi:10.1088/0963-0252/18/1/014015

Wall interactions with plasma generated by vacuum arcs and targets irradiated by intense laser beams

Isak I Beilis

Electrical Discharge and Plasma Laboratory, School of Electrical Engineering,
Fleischman Faculty of Engineering Tel Aviv University, PO Box 39040, Tel Aviv 69978, Israel

Received 11 August 2008, in final form 26 September 2008
Published 14 November 2008
Online at stacks.iop.org/PSST/18/014015

Abstract

The theory of plasma–wall interactions in vacuum arc spots and in laser irradiated spots is reviewed in light of Langmuir's fundamental contributions to the theory of plasmas, sheaths, evaporation and electron emission. The mechanisms of plasma generation in the electrode and laser–target vapors are described. Models of sheath structures at surfaces which emit vapor and electrons are presented and the influence of the relation between the rates of electron and vapor emission on the electrical current continuity at the plasma–electrode boundary is discussed. The mechanisms of current continuity in the vacuum arc anode region, in the short vacuum arc, and in transient cathode spots are described. The important role of the near-target sheath in laser generated plasma is shown, indicating the effect of converting laser radiation absorbed in plasma into kinetic and potential energy of charged particles that impinge on the target. The description is summarized showing that understanding these phenomena relies on Langmuir's pioneering work.

(Some figures in this article are in colour only in the electronic version)

1. Introduction

Plasma is an ionized gas and comprises an assembly of atoms, ions and electrons. Astronomical objects (stars and interstellar matter), natural phenomena (lightning, ball lightning) and the ionosphere contain naturally occurring plasma. In the laboratory, plasma was generated using various types of electrical discharges: glows, sparks, arcs, etc. The earliest research studied the characteristics of the ionized gas in these discharges, including the electric field, potential distribution in the space charge regions near the walls and in the gas volume and voltage–current characteristics.

The space charge region in a discharge with a hot CaO cathode was studied by Child in 1911 [1] taking into account only the case where conduction was solely by positive ions. Langmuir studied the space charge due to electron current in order to understand the difference between measured thermionic currents in a high vacuum and Richardson's saturated electron current [2]. As a result, the dependence between current density, gap voltage and gap distance was obtained, yielding the well-known Child–Langmuir formula. Langmuir later investigated the thermionic current limited by the space charge for coaxial cylinders [3] and concentric spheres [4]. The effect of the initial electron velocity on the potential distribution and thermionic current was investigated previously for parallel plane electrodes [5].

These investigations considered the case where the space charge region length was comparable to the interelectrode gap distance. However, when a relatively small cylindrical or spherical electrode is immersed in an ionized gas, the size of the surrounding space charge region is significantly smaller than the size of the interelectrode ionized gas. In these cases, the space charge region closely surrounding the electrode was called a 'sheath' by Langmuir and was studied to develop a method to investigate the potential, temperature and density distribution in the ionized gas of electrical discharges. The method interpreted different parts of the measured voltage–current characteristic of a small 'collector' electrode immersed in a gas discharge, using the sheath theory [6–8]. This 'Langmuir probe method' is used even currently.

When the sheath is much smaller than the interelectrode gap, the ionized gas contains ions n_i and electrons n_e in about equal numbers so that the resultant space charge is very small. This 'quasi-neutral' region, where the ion and electron charges

are balanced, was first named 'plasma' in 1928 by [9]. Quasi-neutrality prevails at a distance from the sheath where charge fluctuations are not observed and $n_i = n_e$ can be assumed. Langmuir proposed an analogy to phenomena in electrolytes described by Debye and Huckel [10] to determine this distance. The quasi-neutral approximation is not valid within a Debye radius of an electrode, probe or other perturbing body.

Langmuir [9] showed that, if throughout a volume much larger than a Debye radius, the electron density changed by some transient external means, the resulting electric fields act in the direction so as to equalize the density, but the potential energy of these fields is converted into kinetic energy of the electrons so that oscillations occur, and electric waves may result. Presently this phenomenon is widely known as Langmuir plasma oscillations. The interaction of an emitted electron beam with plasma oscillations explains the observed effect of anomalous electron beam energy relaxation to background plasma particle energy distributions [11, 12]. When an energetic, charged particle beam is injected into a plasma volume, the average energy (i.e. temperature) of the background plasma particles is increased, not only due to collisions but also by the beam–plasma oscillation interaction.

Langmuir's analysis of electron and ion motions in the sheath and in the gas volume explains various aspects of electrical current in gas discharges [13]. He showed that the limiting electron current is higher when there is an ion space charge (and hence an ion current) in the sheath and a maximum in the potential distribution in the plasma volume was found, taking into account ions generated by atom ionization in the interelectrode gap. Langmuir summarized a general theory of electrical current in low pressure gas discharges [13].

A theory of the arc plasma was developed by Tonks and Langmuir in 1929 [14]. To describe the arc plasma, five relationships including charged particle balance in the plasma, equations for ion current, ion generation, mobility and plasma energy balance were proposed. These equations had five variables: the electron density, electron temperature, rate of ionization, ion current and axial electric field. This approach described the charged particle behaviour in the arc plasma between the electrodes.

Thus, a brief review of Langmuir's pioneering work shows first of all his very significant contribution to the understanding of plasma–wall and plasma–electrode phenomena. The plasma–sheath potential distribution was obtained for plane, cylindrical and spherical plasmas, for short, intermediate and long mean free path lengths and for different ionization rates. In gas discharges with hot cathodes, the current is limited by the cathode space charge sheath and by the ion flux flowing from the plasma toward the cathode sheath. The initial velocities of the ions and electrons entering the sheath from the gas influence the electron current. The potential distribution in the cathode sheath–plasma and the electron temperature both determine the motion of the ions and thus the ion flux which flows to the cathode sheath. The potential in the anode sheath may be positive or negative relative to the plasma, depending on the anode size. Surface phenomena such as surface–particle interaction and electron emission from metallic cathodes were described theoretically; this theory details thermionic and field electron emission. The above and other important results constitute a useful background for studying plasma in the future and at present allow characterization of modern plasmas.

Below we review progress in understanding phenomena in plasma comprising vaporized electrode and wall material generated by discharges and by laser irradiation, based on Langmuir's results. Such plasmas are generated in particular in vacuum arcs, and when targets are irradiated with high power flux laser beams. Lessons learned from studying the vacuum arc are applicable in understanding vacuum arc deposition of thin films and coatings, vacuum interrupters and other switching devices, vacuum arc remelting and degassing of metals and also pulsed plasma thrusters, capillary discharges, rail-gun accelerators, unipolar arcs in tokamaks and discharges in MHD power generators. The most important phenomena are emission of atoms and their subsequent ionization, emission of electrons and the boundary between the condensed matter and the plasma. These phenomena will be reviewed in the light of Langmuir's work. It will be shown that sheath phenomena control plasma generation in various vacuum arc modes and during laser irradiation.

In this review, evaporation phenomena and the kinetics of metal vaporization are considered in section 2, the plasma–wall transition in section 3 and electron emission in section 4. In section 5, a model of the vacuum arc cathode spot is presented, and the mechanism for maintaining current continuity across the metal–plasma boundary with cathode materials having a range of thermophysical properties is discussed. Other interesting cases are considered, including arcs with large rates of current rise (section 6), transient spots on protrusions (section 7), anode spots (section 8), short arcs (section 9), spot motion in a transverse magnetic (section 10) and laser–target interaction (section 11) and finally the results are summarized in section 12.

2. Solid material vaporization

Langmuir [15] considered a metal surface in equilibrium with its saturated vapor, when the rates of evaporation and condensation are balanced. In general, this balance depends on surface phenomena—condensation, evaporation and atom reflection [16]. Assuming that the rates of evaporation and condensation are equal, the rate of metal evaporation W_L (atom cm^{-2} s^{-1}) into vacuum is determined by the equilibrium vapor pressure P (Torr) [17] as

$$W_L = \frac{P}{\sqrt{2\pi m k T_0}}, \tag{1}$$

where m is the atom mass (in g), k is Boltzmann's constant and T_0 (K) is the surface temperature. Equation (1) is applicable for relatively low temperatures when $P \leqslant 1$ Torr, when the evaporated material flows into the surrounding space without collisions. With increasing T_0, some atoms flow back to the surface due to collisions, and therefore the net rate of material evaporation is less than that given by equation (1). Knudsen [18] showed that for strong evaporation a kinetic treatment is required due to non-equilibrium effects. While a dense vapor flow can be treated hydrodynamically for

relatively large distances from the surface, within a region in the immediate vicinity to the surface the collisions are rare, and a non-equilibrium layer of several mean free path lengths forms, through which atoms are returned back to the surface. The particle velocity distribution function (DF) approaches equilibrium in this *Knudsen layer* or *atom relaxation zone*. Collisions in the vapor relax the DF towards a Maxwellian form. Thus two regions appear near the surface: (i) a non-equilibrium region with rare collisions and (ii) a collision dominated region with hydrodynamic vapor flow. A kinetic approach was used to solve the Boltzmann equation to determine the flow parameters (density n, temperature T and velocity v) in the non-equilibrium region. The parameters at the external boundary of the Knudsen layer determine the boundary condition for the hydrodynamic region, for the flow along a path from the surface. In general, the Boltzmann equation is

$$\frac{\partial f}{\partial t} + \boldsymbol{v}\frac{\partial f}{\partial \boldsymbol{r}} = \left(\frac{\mathrm{d}f}{\mathrm{d}t}\right)_{\mathrm{col}}, \tag{2}$$

where $\boldsymbol{v}$ is the velocity vector, $\boldsymbol{r}$ is a spatial coordinate and f is the DF. The collision term was modeled by Bhatnagar *et al* (BGK) and their approach is simplest for the present case of sharp variation of the vapor parameters near the wall [19]:

$$\left(\frac{\mathrm{d}f}{\mathrm{d}t}\right)_{\mathrm{col}} = \frac{f_0 - f}{\tau}, \tag{3}$$

where f_0 is the local equilibrium DF and τ is a constant collision time. The approach using equation (3) is called the relaxation model. In most practical cases, the characteristic time of the hydrodynamic parameter set is smaller than the characteristic time of the heat flux change to the surface [20]. This allows formulation of a steady state one-dimension equation

$$v\frac{\partial f}{\partial x} = \frac{f_0 - f}{\tau} \tag{4}$$

to which the following boundary conditions must be imposed:

$$f_0 = n_0\left(\frac{m}{\pi 2kT_0}\right)^{3/2}\exp\left[-\frac{mv^2}{2kT_0}\right] \qquad \text{at } x = 0, \tag{5}$$

$$f_\infty = n_\infty\left(\frac{m}{\pi 2kT_\infty}\right)^{3/2}\exp\left[-\frac{m}{2kT_\infty}((v_x - u)^2 + v_y^2 + v_z^2)\right]$$

on the equilibrium side.

The evaporated atoms have a half-Maxwellian DF (f_0) characterized by T_0 and a given density [21], and this DF served as the boundary condition at the evaporated surface, i.e. at $x = 0$. At the equilibrium side the Maxwellian DF (f_∞) is shifted by velocity u. Equation (4) with boundary conditions (5) was solved using different approaches [22]. Anisimov considered the Knudsen layer as a discontinuity surface in the hydrodynamic treatment of the vapor expanding from laser irradiation of a solid [23], similar to earlier treatments of the shock wave problem [24]. Assuming that the velocity at the external boundary of the Knudsen layer is the sonic velocity $u = u_{\mathrm{sn}}$ (i.e. Mach number $M = 1$), Anisimov [23] obtained that the evaporated atom flux is about 0.82 W_L. Fisher [25] solved the kinetic problem using the BGK approach and obtained that the rate of evaporation into an infinite half-space is about 0.85 W_L. Electrode vaporization into plasma taking into account the electron emission also was treated kinetically by Beilis [26–28] (see below). It was found that the plasma flow is impeded when $M < 1$ and the plasma flowed freely into the surrounding vacuum when $M = 1$ [27, 28]. A strongly impeded mass flow was obtained during evaporation in vacuum arc cathode spots due to electrical current and energy dissipation in the dense cathodic vapor plasma and it was found that the vapor flux into current carrying plasma differs from the flux W_L calculated with Langmuir's formula (equation (1)). The condition for impeded plasma flow was studied in the case of the Teflon propellant in thrusters [29, 30].

3. Plasma–wall boundary region

The region bounding a condensed matter object (e.g. electrode, probe, insulating wall) in contact with a vacuum arc plasma usually consists of a collisionless space charge sheath and a quasi-neutral bulk plasma and a transition region between them. The initial ion velocity at the sheath edge was formed in the transition plasma region. Langmuir [13] studied the ions velocity at the sheath edge and stated that 'we must recognize that the velocities of the ions which are measured by E_{p} (i.e. the kinetic energy corresponding to the potential E_{p}) are derived from the weak fields that extend from the sheath a considerable distance into the plasma'. Later Bohm [31] shoved that the ion velocity V_{i} is determined by the electron temperature T_{e} and proposed the condition $V_{\mathrm{i}} = (T_{\mathrm{e}}/m_{\mathrm{i}})^{0.5}$ for a stable sheath at a negatively charged wall. Here T_{e} is in eV.

To theoretically describe the plasma–wall boundary region, the equations of conservation of particle density, the potential and electric field at the sheath–plasma interface should be taken in account to solve the Poisson equation. To this end, Lam [32] proposed an asymptotic analysis considering the Langmuir probe problem. Franklin and Ockendon [33] contributed significantly to developing an asymptotic method of matching the solutions of the plasma and sheath regions in a low pressure discharge. The hydrodynamic approach was considered by Valentine [34] and Riemann [35, 36]. The large importance of the problem encouraged much research [37–43] which analyzed the plasma under various conditions, including determining the relation between the mean free path of different charged particles and the Debye length, in order to understand the potential and electric field distribution. A comprehensive review of recently published works was presented by Franklin [44].

The plasma–wall boundary region in an oblique magnetic field was studied assuming a Boltzmann distribution for electrons [45, 46]. Later the problem was solved without assuming that the electrons were distributed according to the Boltzmann law [47, 48]. It was first shown that when the magnetic field is parallel to the wall, the electron density may deviate from Boltzmann's law. Moreover, even in the case where the obtained plasma density dependence on the electrical potential can be approximated by the Boltzmann distribution, the presheath thickness deviates from that calculated using a model based on such a density distribution.

A model of the smooth transition between the quasi-neutral plasma and the collisionless sheath in which the ion velocity and electric field at the interface are determined self-consistently was proposed [49]. The dependences of the ion velocity and electric field at the interface on the Debye length to the collision mean free path ratio are calculated.

The important parameter to describe the cathode phenomena in an electrical arc is the electric field at the cathode surface. Langmuir's analysis [13] enabled Mackeown [50] to obtain an expression for this field which took into account both the cathode electron emission current and ion current towards the cathode. The model was extended to include the influence of the initial particle velocity, multi-charged ions and the returned flux of plasma electrons [51]. The self-consistent solution of the cathode spot problem showed that the sheath structure depends on the cathode material properties (see section 5).

4. Electron emission

According to Compton's calculations [52], the observed current density in the cathode arc spot is from thermionic emission (T-emission) of electrons. The T-emission electron current was calculated by the Richardson equation using Langmuir's coefficients for carbon and tungsten cathodes where the temperature was relatively high. However, the thermionic mechanism did not explain the data for arcs with relatively cold cathodes, e.g. Cu and Hg. To solve this problem, Langmuir [5, 6, 53] indicated that there is a large electric field at the cathode surface due to the positive space charge of ions and proposed a mechanism known as electron field emission (F-emission). Later, the simultaneous and synergetic contributions of both T- and F-emission, T-F emission, was calculated [54]. Dolan and Dyke [55] calculated the energy distribution of the emitted electrons taking into account the Fermi–Dirac electron distribution in metal and a transmission coefficient of electrons through the surface potential barrier in the form given by Sommerfeld and Bhette for different temperatures T and electric fields E. Beilis [56] extended this method for a wide region of T- and F-emission, showing a transition from T- to F-emission types and an intermediate case. The electric field was also determined when electron emission cooling exceeds resistive heating due to the Nottingham effect (electron emission by tunnelling below the Fermi level) [56].

In the case of extremely large electric fields ($\sim$100 MV cm^{-1}) formed at protrusions, resistive heating due to the high electron current density causes unstable F-emission. This effect was discovered studying the electron field emission from a protrusion in an electron beam source [57]. After some time delay the protrusion exploded and electrons were emitted from the expanded explosive plasma. Explosive electron emission (EEE) was described by Mesyats and co-authors [58]. It was shown that EEE takes place for a certain rate of energy input in the protrusion ($\sim j^2 t$) at a relatively large current density of electron F-emission ($\sim 10^9$ A cm^{-2}) and a short time before explosion ($\sim$1 ns). It should be noted that sometimes the shunting discharge due to gas desorption or metal vaporization at the heating stage can prevent explosion phenomena as it was showed by the study of the wire explosion [59].

5. Vacuum arc: specific cases

The vacuum arc is very interesting because of both the diverse and tightly linked physical processes occurring therein and its important industrial applications [60]. It produces a highly ionized and high velocity plasma jet [61], which is used as a metallic plasma and ion source for coating and thin film deposition and implantation [60, 62]. Recently the vacuum arc micro thrusters capable of providing orbit transfer for spacecraft with mass on the order of a few tens of kilograms or smaller [63, 64] have been investigated. It has high pulse stability, high repetition rates and low-energy consumption per ionized metal mass due to the low ionization energy of metallic atoms.

Only a small portion of the vacuum arc cathode area contacts the plasma region; electrons are emitted only from this portion. Sufficient fluxes of electrons and atoms must be emitted from this portion for self-sustained current continuity. This portion of the cathode surface appears as bright spots known as *cathode spots* [60, 65, 66]. The number of cathode spots is generally proportional to the arc current and varies with material.

The cathode spots move on the cathode surface [66]. Their motion on bulk cathodes consists of discrete jumps while the motion was continuous on thin film cathodes [65]. Spot motion is caused by the removal of the material under the spot, i.e. the metallic film on thin film cathodes, or protrusions on bulk cathodes. The discrete motion on bulk cathodes is related to the spot lifetime. The spot motion appears to be a random walk; when a spot 'dies', a new spot is 'born' at an adjacent location spot [65]. The life cycle of the cathode spot is determined by the cathode surface structure and thus the cathode spot motion on the bulk cathode can be calculated as a statistical phenomenon. Spot types were classified [51, 65] according to the spot velocity V_s, spot lifetime t and spot current I. The time-dependent phenomenology of cathode and anode spots as well as their parameters (e.g. current, velocity and erosion rate) was observed and described [51, 65, 66]. The conducting region is considerably constricted and hence the current density is very high at the cathode spot. The cathode spot region includes the hot cathode surface which emits vapor and electrons and the dense plasma near the cathode from which the plasma jet expands into the ambient space. There are several phenomena such as atom ionization, cathode and plasma heating and a large electric field at the cathode surface due to the positive space charge of the ion flux to the surface. The electron current in the cathode plasma and in the plasma jet to the anode closes the electrical circuit. The current continuity mechanism in the cathode region is quite complicated.

Considering current near the electrodes, the following questions must be addressed: *What is the mechanism of constricted current continuity at the interfaces between the low conductivity plasma and the high conductivity metallic anode and the cathode? How does the evaporation rate into a current-carrying plasma differ from the evaporation rate into vacuum? What is the mechanism of electron transport from the cathode to the plasma for cathode materials with strongly different thermal properties?*

5.1. General spot model

The first systematic descriptions for the cathode spot phenomena on materials with intermediate thermophysical properties such as Cu were developed by Lee and Greenwood [67] using a system of equations with arbitrary parameters, by Ecker [68, 69] using the existing diagram method (region of $T - j$ limited by some conditions for cathode and plasma energy balances), and by Beilis *et al* [70] considering cathode plasma phenomena that allowed them to propose a system of equations without arbitrary parameters [71, 72]. The limitations of Ecker's model was discussed by Beilis and Lyubimov [73] and by Ecker [74].

Observations of the vacuum arc and the erosion traces left on the cathode surface after arcing show that the arc is an intense concentrated energy source. The observed narrow luminous zone above the spot indicates a high current density in the cathode spot, of the order of 10^5 A cm^{-2} or higher, and hence high plasma density, above 10^{19} cm^{-3}. A theoretical model of the cathode spot must consider (i) the specific energy balance at the cathode, (ii) the mechanism for ion transport toward the cathode in the near-cathode plasma and (iii) the mechanism of electron emission.

An analysis of plasma parameters adjacent to the cathode allows building a model [70, 72] that includes a relaxation zone in which the electron beam, emitted from the cathode and accelerated through a space charge (ballistic) zone near the cathode surface, collides with plasma particles and dissipates energy. The kinetic energy of the beam electrons is so high that the length of this relaxation zone, where plasma heating and atom ionization take place, is much greater than the mean free path of the ions. Therefore the ion flux toward the cathode could be calculated on the basis of the hydrodynamic equations for a three-component (neutral, ion and electron) plasma. This permits calculation of the ion current fraction at the surface, thus closing mathematically the system of equations [70].

Two types of heat sources in the cathode enter into its energy balance: (1) the ion and back electron fluxes toward the cathode generate heat fluxes to the surface and (2) the high current density produces volumetric Joule heating in the cathode body. Solving the energy balance equation elucidates the relative roles of the volumetric and surface heat sources, depending on the spot size that is unknown beforehand and is obtained by solution of the system of equations.

In general, the near-cathode plasma pressure deviates from equilibrium and the outflow velocity of particles from the ionization region to the electrode gap plays an important role. The directed flow of erosion products is equal to the difference between the flow of atoms emitted from the cathode and the back flow of heavy particles (atoms and ions) from the plasma. Most of the particles returning to the cathode originate from a non-equilibrium Knudsen zone [28, 75] having a length of a few mean free paths. The velocity DF of the particles approaches equilibrium at the external edge of this layer. In order to determine the particle back flow and thus the net of cathode evaporation (erosion rate in vapor state), the jump in plasma density and temperature in the Knudsen layer was analyzed in a kinetic model [28, 51], which considered, along with the kinetics of heavy particle evaporation, the kinetics of electron evaporation [76]. There are two groups of electrons in the relaxation zone [72]: beam of emitted electrons from the cathode and slow plasma electrons. In this zone there is a large energetic electron flux and a deviation from equilibrium, similar to the case of atom evaporation with a discontinuity in the density and temperature. This discontinuity is enhanced by the space charge sheath, which accelerates the emitted electrons and slows down plasma electrons backstreaming toward the cathode.

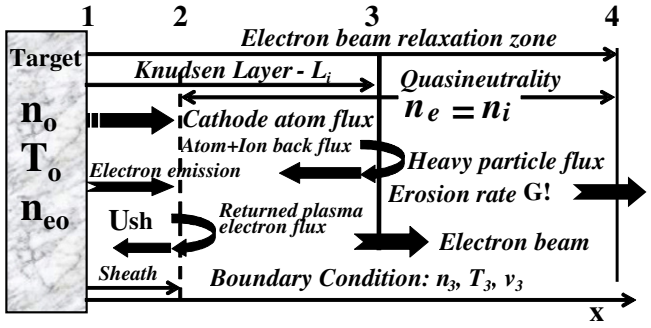

Figure 1. Structure of kinetic layers in the cathode current-carrying plasma.

There are four boundaries in the near-cathode region (figure 1). We define a coordinate system with its origin at the spot centre and the x-direction normal and out of the cathode surface. Boundary 1 is at the cathode surface ($x = 0$), boundary 2 is at the external boundary of the space charge sheath (or ballistic zone), boundary 3 is at the distance of the Knudsen layer length for the heavy particles and plasma electrons from the cathode surface and boundary 4 is located at a distance equal to the emitted electron beam relaxation length from the cathode surface. The gas parameters at these boundaries are denoted as $n_{\alpha j}$, $v_{\alpha j}$ and $T_{\alpha j}$, where the index $\alpha = e$, i, a denotes electrons, ions and atoms, respectively, index $j = 1, 2, 3, 4$ denotes the boundary number and n_{eo} and n_{o} are the equilibrium electron and heavy particle densities determined by the cathode surface temperature T_{o}. The problem is reduced to integrating the conservation equations at the above boundaries as moments of known velocity DFs in the following form:

$$\int v_x f(\boldsymbol{v})\,\mathrm{d}\boldsymbol{v} = C_1; \quad \int v_x^2 f(\boldsymbol{v})\,\mathrm{d}\boldsymbol{v} = C_2;$$

$$\int v_x \boldsymbol{v}^2 f(\boldsymbol{v})\,\mathrm{d}\boldsymbol{v} = C_3, \tag{6}$$

where $f(\boldsymbol{v})$ is the velocity DF at the boundaries, $\boldsymbol{v}$ is the velocity vector, v_x is the velocity component in the x-direction and C_1, C_2 and C_3 are the results of the integration.

If the ionization length and plasma velocity are small in comparison with the length of the relaxation zone and the thermal velocity, respectively, then at boundary 4 Saha's equation is valid [70], i.e. $n_{\mathrm{e}4} = n_{\mathrm{es}}$, where n_{es} is the equilibrium electron density. In the opposite case, an additional diffusion equation [70, 72] determines the ion density at boundary 3, closing the above system of equations. The electron energy balance is determined by energy influx from the emitted electrons and energy dissipated

by ionization, convective transport by the electric current and ion outflow in the relaxation zone. The cathode energy balance determines T_0 and includes cathode heating by ion and electron bombardment of the cathode and Joule heating of the cathode body. The cathode is cooled by thermal conduction, electron emission, evaporation and radiation (according to the Stephan–Boltzmann law [51, 70]). In order to determine the equilibrium parameters at the cathode surface, it is necessary to supplement the system of kinetic equations with an equation for the heavy particle density n_0, determined by the Langmuir equation (1) and the equation of electron emission. The equation of electron emission in a general form is obtained by integrating the second moment of the electron energy function distribution in the cathode, taking into account the transmission coefficient of electrons through the surface potential barrier [51, 56]:

$$j_{\rm em} = \frac{4e\pi m_{\rm e}kT_0}{h^3}\int_{-\infty}^{\infty}\frac{\ln[1+\exp(-\varepsilon/kT_0)]\,{\rm d}\varepsilon}{\exp[6.85\times10^7(\varphi-\varepsilon)^{3/2}\theta(y)/E]}, \tag{7}$$

$$\theta(y) = 1 - y^2\left(1 + 0.85\sin\left[\frac{1-y}{2}\right]\right);$$

$$y = \frac{(e^3E)^{1/2}}{|\varepsilon|},$$

where φ is the work function and $\theta(y)$ is an approximation of the Nordheim function [51, 56]. Equation (7) describes the electron emission dependence on the cathode temperature and the electric field E at the surface. An equation for the electric field was obtained solving the Poisson equation, assuming that the volume charge is formed by positive multi-charged ions with charge state z and also by electrons (emitted from the cathode and backstreaming from the plasma) having a Boltzmann distribution in the sheath [51]:

$$E^2 - E_0^2 = 16\varepsilon_0^{-1}\left(U_{\rm c}\frac{m_{\rm e}}{e}\right)^{1/2}\left\{j_{\rm i}\left(\frac{m}{m_{\rm e}}\right)^{1/2} \times \exp(0.5)\left[\sum_1^z\left(\left(1+\frac{T_{\rm e}}{2zeU_{\rm c}}\right)^{1/2} + \left(\frac{T_{\rm e}}{2zeU_{\rm c}}\right)^{1/2} - \left(\frac{T_{\rm e}}{2eU_{\rm c}}\right)^{1/2}\left(1-\exp\left(-\frac{eU_{\rm c}}{T_{\rm e}}\right)\right)\right)\right] - j_{\rm em}\right\}. \tag{8}$$

It can be seen that E is determined by the ion and emission electron current densities, $j_{\rm i}$ and $j_{\rm em}$, by the cathode potential drop $U_{\rm c}$ in the sheath and by the electron temperature $T_{\rm e}$, eV.

In this formulation, the current per spot is a given parameter while the cathode and plasma parameters at the mentioned boundaries, including the cathode potential drop, are to be determined. The erosion rate can be obtained as

$$G = mn_3v_3, \qquad m = m_{\rm i} = m_\alpha, \qquad n_3 = n_{\alpha 3} + n_{\rm i3}. \tag{9}$$

The electrons transport momentum and energy flux across the sheath. Their flux depends not only on the gasdynamic parameters but also on the height of the potential barrier, i.e. on the cathode potential drop. Thus, the proposed model determines the cathode potential drop and defines the near surface flow regime. Also, the plasma flow is divided into two basic regions: kinetic (before boundary 3) and hydrodynamic (after boundary 3). The kinetic solution yields a relation between the equilibrium parameters $n_{\rm e0}$, n_0 and T_0, and the non-equilibrium plasma parameters at boundary 3 can be obtained (see below). Subsequently the plasma parameters at boundary 3 serve as boundary conditions for hydrodynamic equations of mass, momentum and energy in the expanded plasma jet (see [75]).

Thus the above-described model predicts the spot plasma parameters, cathode erosion rate, spot radius, i.e. the spot current density and the cathode potential drop for the given spot current. The spot motion is determined by the spot lifetime on the local place on the cathode surface. This lifetime is limited by a sharp cathode potential rise due to large cathode energy losses with the time of spot operation. The spot motion mechanism is determined by the cathode energy balance and depends on the cathode surface state and cathode type (bulk or film) and thermophysical properties of the cathode materials. The details of spot motion and arc voltage fluctuation mechanisms were considered in [65]. Below the spot parameters will be discussed separately for cathode materials with intermediate, refractory and volatile thermophysical properties.

5.1.1. Intermediate cathode materials. For intermediate cathode materials such as Cu, Al, Ni and Ti, the electron emission flux is comparable to the evaporated atom flux for a wide region of cathode temperatures. This means that the heated cathode emits vapor and electron fluxes in a proportion such that the reproduced plasma density can support the self-consistent spot operation. As an example, the spot parameters were calculated for Cu and Ti cathodes with spot currents I = 1–20 A [66]. The calculation for the I = 5 A, 1 ms duration yielded T_0 = 4200 K (Cu) and 3600 K (Ti), heavy particle density $n_T = (n_{\rm a} + n_{\rm i}) = 2\times10^{20}\,{\rm cm}^{-3}$ (Cu) and $3\times10^{18}\,{\rm cm}^{-3}$ (Ti), spot radius 9 μm (Cu) and 68 μm (Ti), degree of ionization α = 0.9 and 0.99, $T_{\rm e}$, = 2.7 eV (Cu) and 1.84 eV (Ti), $E \sim 10^6$–$10^7\,{\rm V\,cm}^{-1}$, electron current fraction $s = j_{\rm e}/j$ = 0.64 and 0.67 and the relation of the plasma pressure P_3 to the equilibrium pressure P_0 0.7 (Cu) and 0.67 (Ti).

The dependence of the steady cathode potential drop $U_{\rm c}$ on the spot current is presented in figure 2 and of the cathode potential drop with I = 5 A on the spot lifetime in figure 3. $U_{\rm c}$ decreases sharply when the spot current and life time increase and is larger for Cu. $U_{\rm c}$ for small current (2 A) and a short lifetime (<1 μs) significantly exceed the measured minimal value for Cu, 15 V [77], possibly explaining the observed potential fluctuations and unstable operation for very small arc currents [77].

The plasma velocity within the cathode spot region is substantially lower than the sound velocity ($v_{\rm sn}$). It is indicated by a relatively small parameter $b_3 = v_3/(2kT_3/m)^{1/2}$ which increased from 0.02 to 0.1 with the spot current. This means that the returning mass flux to the cathode is large and that the plasma flow in the cathode region is impeded ($v_3 < v_{\rm sn}$).

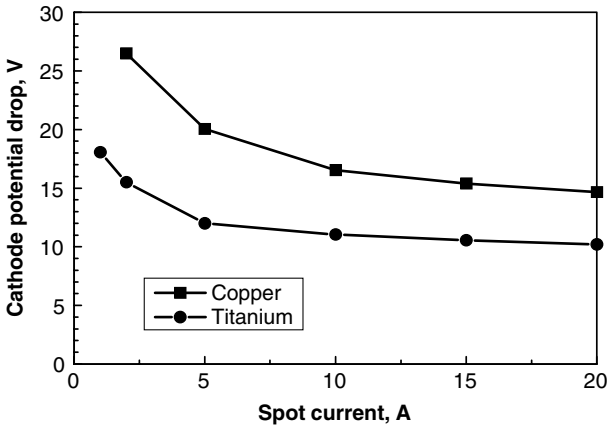

Figure 2. Cathode potential drop as function of the spot current [75].

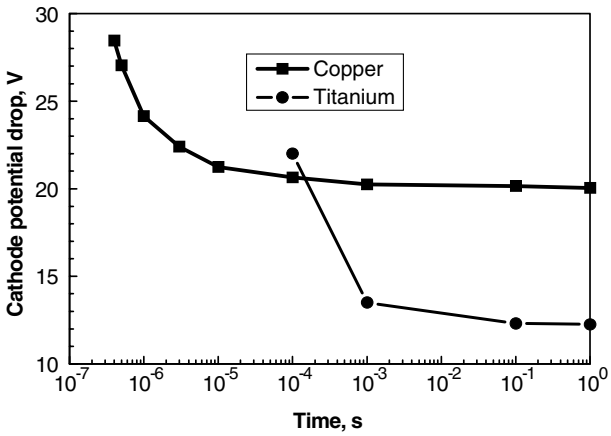

Figure 3. Cathode potential drop as function of the spot life time [75].

The calculation showed that an initial pressure is required for new spot ignition because the evaporated mass flow should be impeded to continue the plasma generation from the initial stage in the cathode region. The calculated cathode erosion rate G ($\mathrm{g\,s^{-1}}$) is about 10% (and lower) of the cathode material vaporized according to the Langmuir–Dushman law in vacuum [78]: $\log G \sim (A - B/T_0)/T_0^{0.5}$, where A and B are constants [78]. The calculated erosion coefficient G_k ($\mathrm{g\,C^{-1}}$) was in the region 70–100 $\mu\mathrm{g\,C^{-1}}$ and agrees with the measured values [79].

5.1.2. Refractory cathode material. The thermophysical properties of refractory materials lead to a large electron emission-to-atom evaporation rate ratio (>10) for a wide range of cathode temperatures T_0 [73, 80, 81]. The cathode spot model which works well with cathodes having intermediate thermophysical properties predicts for refractory cathodes a plasma density that is so small that T_0 cannot be supported by the energy flux in the cathode region [73, 81]. The model was improved by finding a mechanism to reduce the large electron current and increasing the vapor flux-to-electron emission flux ratio. A lower electron current density j_e from the refractory cathode compared with the saturated value is predicted using a 'virtual plasma cathode' [51, 81] (see below). According

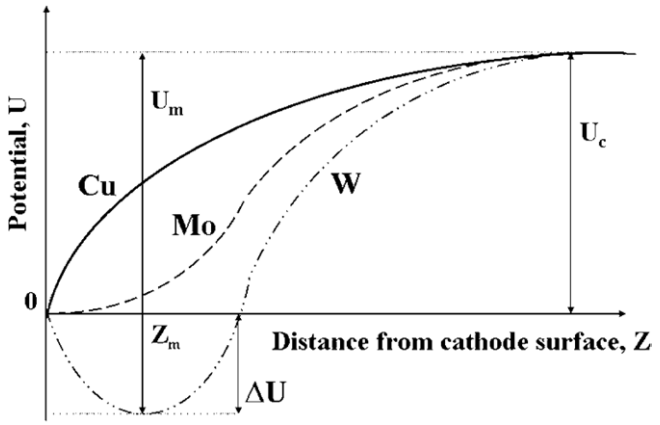

Figure 4. Schematic potential distribution in the cathode sheath for different cathode materials. The distance Z_m of the 'virtual cathode' for W where the potential is at its minimum and the negative value is a consequence of the space charge region which limits the electron emission current, as studied by Langmuir [13] for a space charge limited diode.

to this model, a solution can still be obtained with a very large electron current fraction $s = j_e/j$, approaching 0.99. As the ion current toward the cathode should be of a certain level to heat the cathode, the large s leads to a relatively large total spot current density, $j > 10^6\,\mathrm{A\,cm^{-2}}$ [81]. Large j is usually a characteristic of the non-stationary fast moving spot types [65, 66]. However, in the vacuum arc, slowly moving and steady-state spots with $j < 10^6\,\mathrm{A\,cm^{-2}}$ were observed on tungsten [82–84] and molybdenum [85] cathodes. At the same time, calculations [81] show that lower j is consistent with lower s (<0.8). A question arises: *How does the spot on refractory cathodes operate in a self-sustained manner with a low s? Below an approach will be considered to solve this problem.*

To this end figure 4 presents a schematic potential distribution in the sheath for different cathode materials. For refractory materials, the electron density exceeds the ion density in the sheath adjacent to the cathode and the consequent negative space charge forms a potential minimum U_m with respect to the plasma potential and has a potential difference of ΔU with respect to the cathode. The region with the potential minimum is called the *virtual cathode*. When the virtual cathode approach is used, a zero electric field at the plasma–sheath interface is also assumed [13]. As result, the ratio of emitted electron current density j_e to the incident ion current density j_i is proportional to the square root of the ion mass m to the electron mass m_e ratio, i.e. $j_e/j_i \sim (m/m_e)^{1/2}$ [13, 81]. Thus j_e is much larger than j_i. Mathematical analysis of the sheath shows that the ratio j_e/j_i will be lower if the electric field at the external boundary of the sheath $E_p \neq 0$. The $E_p \neq 0$ condition was from presheath investigations [43, 48] and the maximal field E_p is E_d here that can be estimated as $\sim T_e/L_d$, where L_d is the Debye length. Therefore in the calculated model for the refractory cathode, a non-zero electric field at the plasma–sheath interface and the quasi-neutral plasma consisting of ions with different charge state in the cathode region were taken into account. When the zero

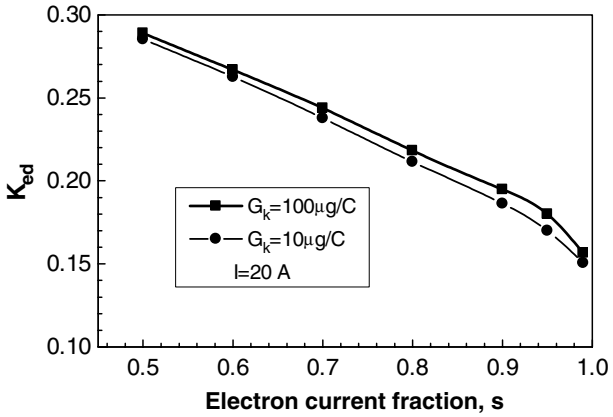

Figure 5. Electric field at the sheath–plasma interface normalized by the ratio of the electron temperature to the Debye length as a function of the electron current fraction in the spot with the W cathode erosion rate as a parameter [22].

potential at the plasma–sheath boundary and the zero electric field at the virtual cathode were taken into account, the solution of Poisson's equation was obtained in the following form [86]:

$$E_p^2 = Aj(1-s)\left[(2e_N)^{0.5}\sum_z f_z((1+\eta_z^{-2})^{0.5}-\eta_z^{-1}) - s_T d - s_e\right], \qquad (10)$$

$$A = (8U_m A_i)^{0.5}/\varepsilon_0, \qquad d=(z\pi/\eta_z)(1-\mathrm{Exp}(-eU_m/T_e)),$$

$$s_T = \varepsilon j_{eT}\mathrm{Exp}(-eU_m/T_e)/j_i,$$

$$\eta_z = (zeU_m/T_e)^{0.5}, \qquad s_e = \varepsilon j_v/j_i, \qquad \varepsilon = (m_e/m)^{0.5}$$

$$K_{ed} = E_p/E_d,$$

where ε_0 is the permittivity of vacuum, e_N is the Napierian base, A_i is the atom weight, s_T is the fraction of returned electrons current density j_{eT}, s_e is the fraction of electron current density j_v emitted by the virtual cathode and K_{ed} is the ratio of E_p to the presheath electric field E_d. ΔU was calculated using the thermionic electron emission current density j_{em} [56, 60] and the electron current density j_v emitted by the virtual cathode as $\Delta U = T_e Ln(j_{em}/j_v)$, T_e is in eV.

Equation (10) shows the relation between E_p, U_m and the electron current fractions. Numerical analysis using equation (10) instead of equation (8) in the cathode spot model shows the relationship between E_p and E_d for different s. To this end, the relation of K_{ed} was calculated as a function of s for $I = 20$ A and $U_c = 20$ V [60], using the spot model with equation (10). Figure 5 shows that K_{ed} decreases with s and reaches ~0.1 for $s > 0.9$. The spot current density j was about 10^5 A cm^{-2} for $s < 0.9$ which agrees with the experimental result [84].

5.1.3. Volatile cathode material. There is a problem, caused by very little electron emission flux in comparison with the vapor flux, for volatile materials, e.g. Hg. A modified model was proposed where an additional plasma layer adjacent to the cathode layer is hypothesized and serves as a 'plasma cathode' supplying electrons for self-sustained arc operation [87].

The near-cathode region was modeled with two distinct regions, divided by a double sheath (figure 6). The plasma cathode (region I) is in direct contact with the cathode surface (boundary 1) and shares boundary 2 with a double sheath (region II). Electrons are created in region I by vapor ionization, and boundary 2 thus serves as a virtual cathode for the rest of the discharge, while current continuity is maintained at boundary 1 mostly by the ion current. Ions are neutralized by electrons at the cathode surface; these electrons close the circuit current and the electrons generated in the plasma of region I flow towards region III through region II. Region II is a collisionless space charge double sheath having a relatively large potential drop (see figure 6) and bounded by boundary 2 which it shares with region I and boundary 3 which it shares with plasma region III which extends to boundary 4 in the anode direction with the length equal to the relaxation length of the electrons emitted from region I.

Two types of time-dependent solutions were found, with characteristics times of 0.1–1 μs and 100 μs, respectively [87]. These times correspond to the experimentally observed spot life times for the transitional (arc voltage 18–21 V) and fundamental arc (arc voltage 9–10 V) forms, respectively, observed by Kesaev [77]. The potential drop in the plasma regions (figure 6) U_1 and U_2, typically <0.5 V, are small in comparison with the double sheath potential drop U_{sh} (10–15 V). The acceleration of electrons from the first plasma region through the layer with potential drop $U_{sh} + U_h$ explains the observation of fast electrons with energy exceeding the measured arc voltage [77]. The calculation shows that U_{sh} can be small (~10 V) in accordance with the measurements for the fundamental form of the Hg arc voltage [77]. The length of the first plasma region is calculated to be 10 μm, which is approximately equal to the experimentally observed dark space in the Hg vacuum arc [77].

6. Arcs with $dI/dt > 10^7$ A s^{-1}

There are specific conditions when multi-charged ion lines were observed spectroscopically [77] and the ion energy becomes significantly larger than the ion energy measured in arcs with low dI/dt or dc. The cathode surface luminosity for currents up to 150 A was investigated with high spatial (~μm) and temporal (~ns) resolution using laser absorption photography [88] with high-speed image converter and streak cameras [89–92]. The periodic fluctuations of the spot brightness, on a nanosecond time scale, were associated with the lifetime of spot fragments. A fragment size of about 10 μm with a lifetime of about 10 ns at a given position and a current per fragment of about 10 A were found with Cu cathodes. The spot operation mechanism with this spot duration and current is the subject of this section.

One proposed model is based on the explosive emission of a microprotrusion on the electrode surface [93]. While the explosion could be initiated by a very strong electric field (~100 MV cm^{-1}), it is problematic to reach it in low voltage arc spots because the electric sheath width is significantly lower

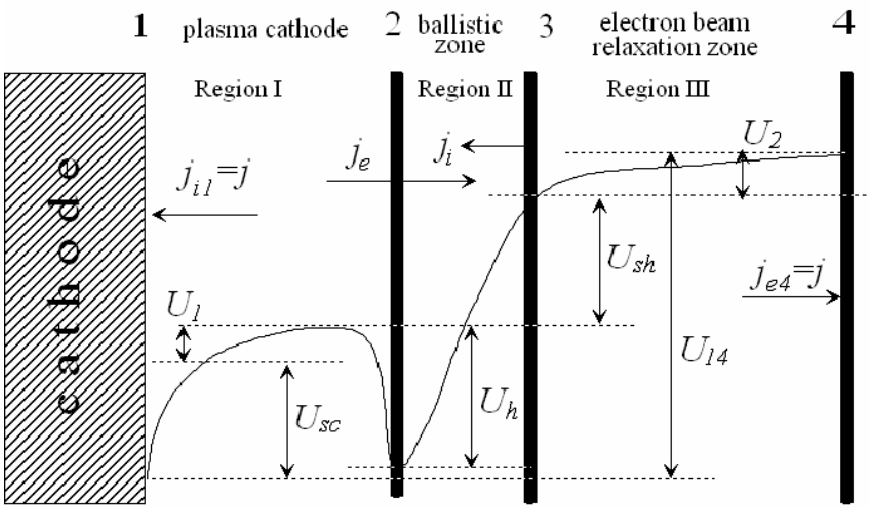

Figure 6. Near-cathode schematic potential distribution for a volatile cathode material: cathode plasma region—I, with screening potential drop U_{sc}, double sheath—II and electron beam relaxation zone—III. U_1 and U_2 are the potential drops in plasma regions I and III, respectively [87].

than the size of the protrusions [51]. If the spot current is $I = 10$ A [89–91] during time $t = 10$ ns, then the rate of spot current rise $\mathrm{d}I/\mathrm{d}t$ is equal or higher than 1 GA s^{-1}. A very important question is: *how is the cathode heated in the spot region*?

To answer this question, the general spot model described above was modified, taking into account the specific cathode energy balance with a relatively large rate of spot current rise. In order to understand the cathode heat balance let us consider the spot current change during the spot life.

6.1. Nanosecond spots on a flat cathode

The main point in the mathematical model of the nanosecond spot is the description of cathode heating, taking into account the transient character of the spot operation due to rise in the spot current in time. Assuming a Gaussian distribution of the heat flux from the spot to the cathode surface and a linear spot current increase with time, the solution of the heat conduction equation was obtained as [94]

$$T_0(t) = \frac{U_{\mathrm{ef}}}{2\pi\lambda}\sqrt{\frac{t}{\pi k_t}}\frac{\mathrm{d}I}{\mathrm{d}t}\left(\frac{\mathrm{d}I}{\mathrm{d}t}\frac{1}{4\pi k_t j}+1\right)^{-1}, \qquad (11)$$

where $T_0(t)$ is the time-dependent cathode surface temperature, U_{ef} is the effective cathode voltage [51, 70] and j is the spot current density. The system of equations for the cathode spot [51] was solved together with equation (11). Figure 7 demonstrates the current density dependence on the rate of current rise. The current density, in general, increases linearly with $\mathrm{d}I/\mathrm{d}t$ and for a characteristic cathode potential drop of 16–20 V, the T-F current density is about twice that of the thermionic emission including the Shottky effect (T-Sh). Numerical analysis showed that field emission begins to contribute at a relatively high cathode electric field when the spot current density exceeds (3–5) $\times$ 10^7 A cm^{-2}.

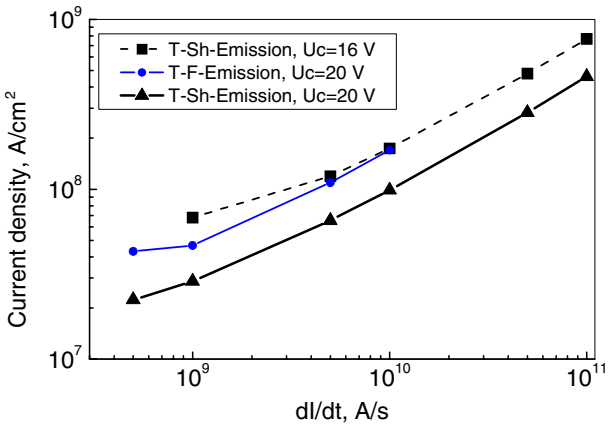

Figure 7. Spot current density versus the rate of spot current rise ($\mathrm{d}I/\mathrm{d}t$) in cases of T-Sh-and T-F-emission, for spot current $I = 10$ A, Cu cathode [94].

In the nanosecond spot, the large current density (10^7–10^8 A cm^{-2}) is supported by a very high electron current fraction (~0.9). Therefore, the incoming heat flux to the plasma causes a high value of T_e (a few electronvolts). In this case, the plasma generates a large flux of hot electrons. Their energy flux together with that of the ion energy flux heats the cathode and thus supports cathode evaporation. The contribution of Joule heating in the cathode is relatively small and agrees with Rich's [95] conclusions for $j < 10^8$ A cm^{-2}.

6.2. Anomalous plasma acceleration

Low-energy ion acceleration (for $I \sim 100$ A and $\mathrm{d}I/\mathrm{d}t < 1$ MA s^{-1} the ion energy is about 100 eV [61]) was associated with a plasma pressure gradient in the cathode plasma jet at a distance of a few spot sizes [51, 65, 96] from the cathode surface. High ion energies (1–10 keV) were measured in microsecond arcs with $I > 1$ kA and $\mathrm{d}I/\mathrm{d}t > 100$ MA s^{-1} [97]. The nature of high energy ions acceleration was explained by the spot model, modified by taking into account

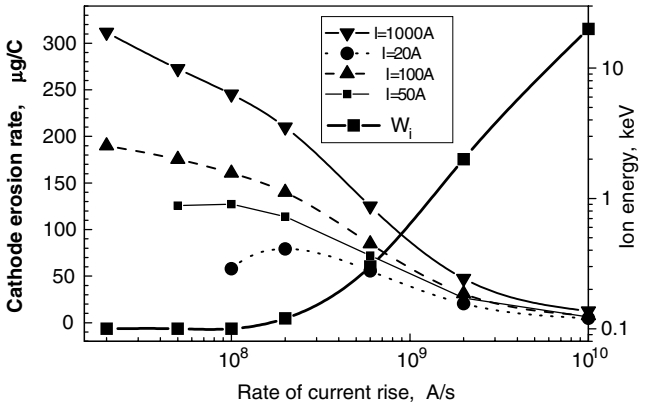

Figure 8. Calculated cathode erosion rate (left axis) and measured ion energy W_i [97] (right axis) as functions of dI/dt for spot current 0.02–1 kA [98].

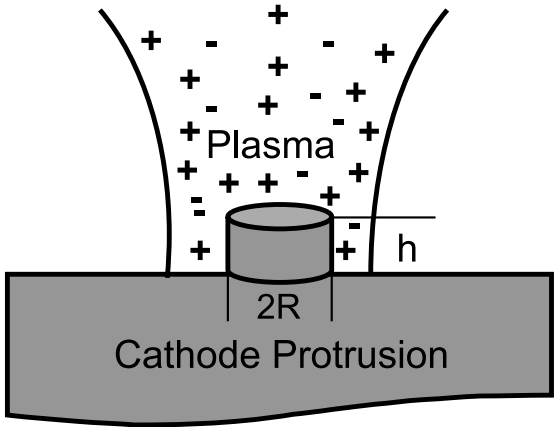

Figure 9. Model of the cathode protrusion with radius R and height h and surrounding plasma.

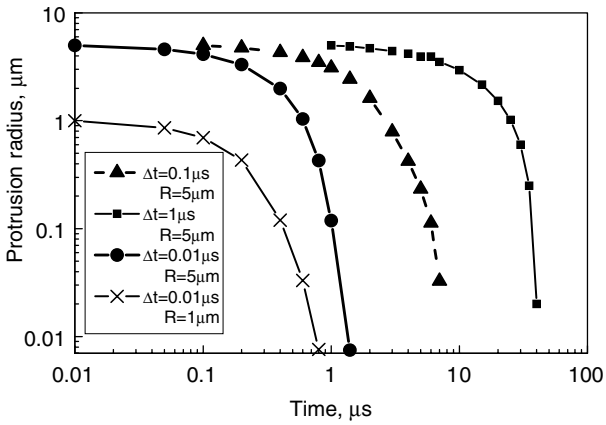

Figure 10. Protrusion size as a function of time ($h = R$) [100].

the cathode energy balance with the spot current increasing during the spot life (equation (11)) [98]. It was shown that the considerable increase in the ion energy in the cathode plasma jet with dI/dt was caused by the increase in the spot plasma pressure and decrease in the parameter eG/m (e is the electron charge, m is the heavy particle mass), which is in essence the ratio of the ion flux to the electron flux [51, 75]. Decrease in eG/m increases the momentum and energy transfer from the plasma electrons to the ions and increases the ion acceleration.

The region of G corresponding to the measured ion energy values was calculated for different spot currents using measured $W_i(dI/dt)$ data [97], where W_i is the ion energy. The results of this calculation for $I = (0.02–1)$ kA and $U_c = 20$ V are presented in figure 8. It can be seen that the cathode erosion rate decreases from about 300 to 10 $\mu g\,C^{-1}$ when the ion energy increases from 0.1 to 20 keV. Note that for this range of ion energy, the value of dI/dt increased [98] from 0.01 to 10 GA s^{-1}, respectively [98].

7. Transient spots on a protrusion

When the spot current is relatively small, the spot sizes can be equal to the characteristic sizes of surface irregularities [51]. The electrical field and high density electron field emission can be supported by a relatively large positive space charge. A self-consistent calculation [99] showed that the plasma density generated by protrusion explosion is too small to support the spot plasma density because it is too a small protrusion when the space charge thickness is much larger than the protrusion size. A question arises when the space charge region is much thinner than the protrusion size: what will be happen to the protrusion when the electric field at the cathode surface is below the critical value for protrusion explosion and the protrusion is heated around by the ion energy flux?

To consider this effect, the cathode spot model described above (section 5.1) was modified to take into account the particular features of the spot appearing on a protrusion, considering for simplicity a cylindrical protrusion with radius R and height h [100], as illustrated in figure 9. To solve the transient self-consistent problem, the initial conditions include the plasma density and temperature which appear immediately after arc ignition or after extinction of a previously operated spot. A step time Δt of initial plasma action the protrusion is defined as time period in which the plasma parameters are constant; after Δt the protrusion size is reduced by its vaporization with a calculated erosion rate. The time-dependent plasma parameters were obtained taking into account the protrusion radius decrease, using a number of time steps during the spot operation, until the protrusion was completely evaporated.

The solution was obtained for different $\Delta t = 0.01$, 0.1 and 1 μs and for $R = h$. As an example, the time-dependent protrusion sizes are presented in figure 10. It can be seen that for all cases, the protrusion radius at first decreases slowly, and then after some critical time, decreases rapidly to zero. The protrusion life time increases with step time Δt and with the initial size of the protrusion. From the solution, it may be concluded that the surrounding plasma heats the protrusion (via ion and backstreaming electron bombardment) to a relatively high temperature which can support self-consistent spot operation, while the electric field is far from the value required for protrusion explosion by volumetric heating by current density due to F- or T-F electron emission. This means that the protrusion is an emission center of plasmas without explosive phenomena.

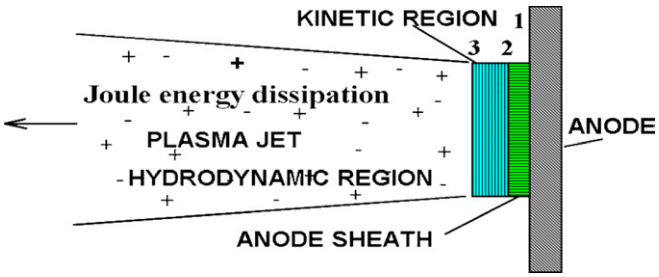

Figure 11. Schematic diagram of the anode plasma region.

8. Anode spot

The transition into the anode spot mode was discussed by Kimblin [101] and Miller [102]. It was established that in vacuum arcs this transition depends on the electrode geometry, interelectrode gap and arc current. A review of the anode spot was presented by Ecker [103] and by Beilis [104]. The anode current density in such anode spots can be 10^3–10^6 A cm^{-2}. Most of the models assumed some free parameters such as anode radius, electron temperature,or arbitrary conditions such as Steenbeck's minimum power principle, pressure balance with self-magnetic pressure in the spot [104]. The anode erosion rate was calculated as evaporation in vacuum using the Langmuir–Dushman relationship [13, 78]. The plasma energy balance was not considered, which is important for understanding the mechanism of plasma electron heating and the degree of ionization. This question was analyzed in the model of [104].

According to the anode spot model [104] the discharge region near the anode consists of (1) a space sheath, (2) non-equilibrium plasma layer and (3) a plasma acceleration region (figure 11). In the hydrodynamic region, the atoms are ionized by plasma electrons. The plasma electrons are heated by the Joule energy dissipation in the current-carrying plasma jet. It is assumed that the heavy particle temperature T in the hydrodynamic region is uniform and equal to T_3, at boundary 3 that is the external boundary of the Knudsen layer in the anode region, figure 11 (the boundaries are defined similar to the definition in the cathode region). Electron temperature T_e differs from T and is assumed uniform in the hydrodynamic region. These assumptions are based on calculations of the plasma particle temperature distributions in the cathode jet, where the mentioned temperatures do not substantially vary [51]. The heavy particle density n_T and velocity v vary from their values n_3 and v_3, respectively, at boundary 3 to their values in plasma jet during plasma acceleration in the hydrodynamic region at boundary 4. In this region, the plasma is quasi-neutral and has a very weak electrical field E_{pl} [51]. The case with a relatively large interelectrode distance was considered, where only a small fraction of the cathode plasma density is in contact with the anode spot area.

Calculations for a graphite anode indicated the following spot parameters for currents of 10–400 A (see [104]). The electron temperature vary weakly and was about 0.55–0.7 eV and the anode spot temperature was in the range 3500–4900 K. The degree of ionization was relatively small: 10^{-3}–5×10^{-2}. This important result can be understood by taking into account the anode current supported by larger electron mobility and lower anode spot electron density than by lower ion mobility and therefore larger ion density in the cathode spot for reaching this same current density.

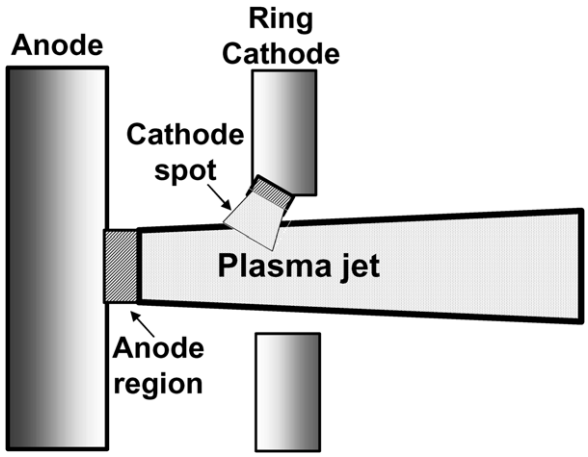

Figure 12. Schematic presentation of the plan anode and ring cathode, cathode and anode regions and plasma jet.

The anode erosion fraction, defined as the ratio between the anode erosion rate to the anode material evaporation rate, was obtained using the Langmuir–Dushman formula [13, 78]. The anode erosion fraction for an anode spot at a given anode surface temperature depends on the anode spot current. It was shown that for $I = 400$ A and in the region of $G = 1$–10 mg s^{-1}, the anode erosion fraction is about 7–25%, while for $I = 10$ A this fraction is larger and for $G = 0.1$–1 mg s^{-1} is about 15–50%. The calculation shows that in the considered ranges of anode erosion rate, spot current and spot lifetime, the anode spot radius is in the range 10–1000 μm.

9. Short vacuum arc

In conventional (large gap) vacuum arcs, the plasma jet is produced in the cathode region using an anode that can be a passive collector of the current. In vacuum, the plasma is accelerated to supersonic velocity at a distance of about 2–3 cathode spot radii ($\sim$10–100 μm [51]) and therefore the arcs can be investigated for micro-plasma generation and for micro-propulsion applications. In microscale devices [105], the plasma is generated by short gap vacuum arcs, where phenomena both in the cathode and anode regions should be taken in account. The short vacuum arc (SVA) with a gap of 1–10 μm and low current ($<$10 A) and short pulse duration (0.3–3 μs) was investigated for contact systems [105–107].

To understand the plasma phenomena in a SVA, a configuration with a planar anode and ring cathode was considered (figure 12) [108]. A model was framed which considered circular anode and cathode spots with different radii and used kinetic models for the cathode [51] and anode [104]. Two erosion fluxes are produced: from the cathode $G_c = m_c n_c v_c$ and from the anode $G_{an} = m_a n_a v_a$, where $m_{c,a}$, $n_{c,a}$ and $v_{c,a}$ are atom mass, heavy particle density and velocity

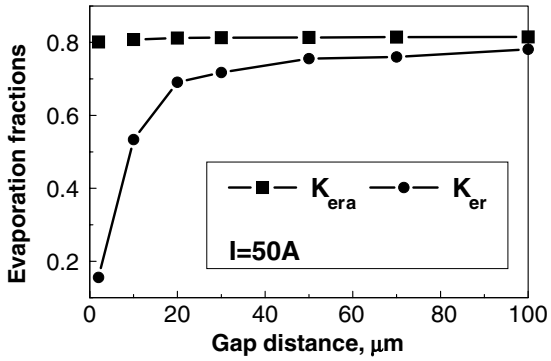

Figure 13. Net of cathode K_{er} and anode K_{era} evaporation fractions as a dependence on the interelectrode distance [108].

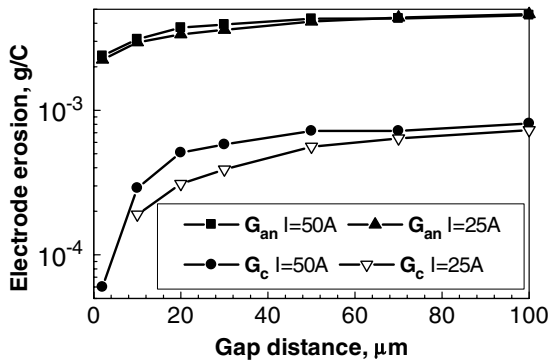

Figure 14. Cathode G_c and anode G_{an} erosion rates in ($g\,C^{-1}$) as a function on the interelectrode distance [108].

for the cathode and anode, respectively. The resulting erosion mass flow G ($g\,s^{-1}$) from both electrodes is $G = G_c + G_{an}$.

The electrode bodies are heated ohmically: (i) the cathode by the incident ions accelerated in the ballistic region (sheath) with cathode potential drop U_c and by the back-flowing electron flux and (ii) the anode by electrons and returned ions from the adjacent plasma. The anode is also heated by a part of the electron beam emitted from the cathode that did not relax in the SVA gap. The ion and electron fluxes toward the cathode and ion flux toward the anode are formed in the ballistic and Knudsen layers. The electrode is cooled by thermal conduction, electron emission and electrode evaporation. The plasma electrons are heated by a part of the electron beam emitted from the cathode that relaxed in the SVA gap as well as ohmically (determined by IU_p, where $U_p = jh/\sigma_{pl}$ is the voltage drop in the gap with distance h, j is the current density and σ_{pl} is the electrical conductivity of the highly ionized plasma). A negative anode potential drop U_{an} is produced when the flux of thermal electrons exceeds the arc current I. The plasma expands into vacuum as a jet and the plasma velocity V is determined by the equations of momentum and energy conservation. The plasma is accelerated by the ion and electron pressures and by electron–ion friction [51].

The calculation conducted for $I = 25$ and 50 A, arc duration $t = 1$ ms, gap $h = 2$–$100\,\mu$m and spot radius $r_a = 2r_c$ indicated that a dense plasma ($\sim 10^{20}\,cm^{-3}$) was formed with mainly singly charged ions and degree of ionization ~ 0.1, $T_e \sim 1$ eV, $U_{an} = -(5$–$6)$ V and $E \sim 10^7\,V\,cm^{-1}$. The cathode spot current density j decreases from 2 to $0.2\,MA\,cm^{-2}$ when h increases from 2 to $100\,\mu$m and j exceeds j_i by a factor of about 3. The anode evaporation fraction K_{era} is significantly larger than K_{er} which increases with h (figure 13) indicating that the anode plasma deviates from equilibrium in the anode Knudsen layer far more than in the cathode plasma. The cathode erosion G_c ($g\,C^{-1}$) increases with h and G_c is much less than the anode one G_{an} ($g\,C^{-1}$), which weakly depends on h (figure 14). The calculated force per current ($G_{an}V$, where V is the jet velocity) in the anode region increases from 3.4 to $4.9\,mN\,A^{-1}$ with distance while this force for the conventional cathodic arc is much lower, about $0.2\,mN\,A^{-1}$ [109]. The calculated large anode evaporation fraction in the short arc does not contradict the measured erosion rate for conventional arc [110]. The calculated relation between G_{an} and G_c was due to the anode temperature significantly exceeding the cathode temperature T_c in the spots. The anode temperature exceeds the cathode temperature because the larger electron current ($j > j_i$) cools the cathode and warms the anode. Thus, the nature of the force and mass flux in SVA was determined by the anode phenomena and they exceed the force and flux generated in a large gap cathodic arc. It was proposed to exploit this important result for SVA micro-thrusters for spacecraft propulsion and micro-plasma sources (see [108]).

10. Cathode spot motion in a transverse magnetic field

An interesting phenomenon occurs when the vacuum arc is operated in a magnetic field—the cathode spots move in the $-\boldsymbol{j} \times \boldsymbol{B}$ direction, i.e. opposite to what would be intuitively expected from Ampere's law [77, 92, 103]. This 'retrograde' spot velocity was measured as a function of the magnetic field, arc current, surrounding gas pressure, gap spacing and cathode material [77, 92]. In vacuum arcs, the retrograde spot velocity increases linearly with the magnetic field and then saturates at the maximal velocity observed during the random spot motion without a magnetic field.

A review of different hypotheses, proposed to explain the retrograde motion, was described [77, 92, 111]. The Beilis model [111] was based on the asymmetric distribution of the magnetic pressure around the spot, taking into account that an initial pressure is required for new spot ignition to fulfil the condition of impeded plasma flow in the cathode region (see section 5.1.1). The self- and external magnetic fields were superimposed, producing a large magnetic pressure on the retrograde side of the spot, hence increasing the probability of new spot ignition in that direction. Thus, the location of the maximum of magnetic pressure affects the regime of plasma flow during the plasma creation in the vicinity of the cathode surface and determines the direction of spot motion [111].

11. Laser–target interaction

Another example of constricted plasma is that generated by high intensity laser radiation of metallic targets. Laser radiation has been used in the last decade for different

applications [112]. For sufficiently high power flux ($>1\,\mathrm{MW\,cm^{-2}}$), the laser beam evaporates and ionizes the material, creating a plasma plume near the target surface. A model [113] was proposed to understand the plasma structure near the target and how the charge particles influence the energy and particle conservation.

The laser generated plasma has similar characteristics to the plasma generated in the cathode region of a vacuum arc [51, 65, 114, 115]. They are both very dense and appear in minute regions, known as laser spots and cathode spots. The cathode spot model was modified for the particular features of a laser generated plasma. It was assumed that the spot is circular with radius R_s and located on a smooth surface. The important issues are the plasma–surface interaction in the spot region, the energy flux to the target by the ions with the ion current density j_i and by the electrons emitted from the hot target surface with current density j_{em}. As in the arc spot, the energy of charged particle fluxes is determined by the potential drop U_{sh} in a sheath adjacent to the target surface. In contrast to the current-carrying vacuum arc cathode spot, the net electrical current is zero in the laser spot (for moderate intensity irradiation), leading to the following equations:

$$j_e + j_i = 0, \qquad j_e = j_{em} - j_{et}, \tag{12}$$

where j_{et} is the current density of back-flowing electrons. Using equation (12), an expression for the potential drop in the sheath U_{sh} can be obtained:

$$U_{sh} = T_e Ln\left(0.6\sqrt{\frac{2\pi m_e}{m}} + \frac{j_{em}}{en_{es}}\sqrt{\frac{2\pi m_e}{T_e}}\right)^{-1}. \tag{13}$$

The electron temperature was determined by the balance between the energy absorbed from the laser with power density q_L and the energy of the emitted electrons, accelerated in the sheath with potential drop U_{sh}, and the energy expended in ionization and the energy outflow by the electron and ion fluxes (with particle fluxes $n_{e4}v_4$ and $n_{i4}v_4$) through the external boundary of the relaxation zone. The coefficient of laser energy absorption in the plasma varies parametrically as indicated in [113, 115]. Plasma quasi-neutrality requires that $n_e = \Sigma z n_{iz}$, where n_{iz} is the density of ions with ion charge $z = 1, 2, 3, 4$ and n_e is the electron density. The plasma pressure is $P_j = \Sigma n_{aj} T_{aj}$ ($j = 3, 4$). The target is heated by laser irradiation that is not absorbed in the plasma, by incident ions (bringing energy flux $j_i U_{sh}$) and by back-flowing electrons with current density j_{et} from the adjacent plasma and cooled by electron emission and thermal conduction into the bulk of the target.

A calculation for a Cu target, irradiated in a spot radius of 100 μm, with pulses of durations 1 ns to 1 ms, with laser power densities of $q_L = 0.001$–$1\,\mathrm{GW\,cm^{-2}}$, showed that U_{sh} was in the 2–25 V range and decreased with q_L and pulse duration (figure 15). The ratio K_{er} of the net evaporation rate to the 'Langmuir flux' (i.e. unobstructed evaporation into vacuum) increased with q_L from 0.01 to 0.4 (figure 16). The electron temperature T_e can reach up to ~5 eV for short (~1 ns) laser pulse duration. The degree of ionization increased with

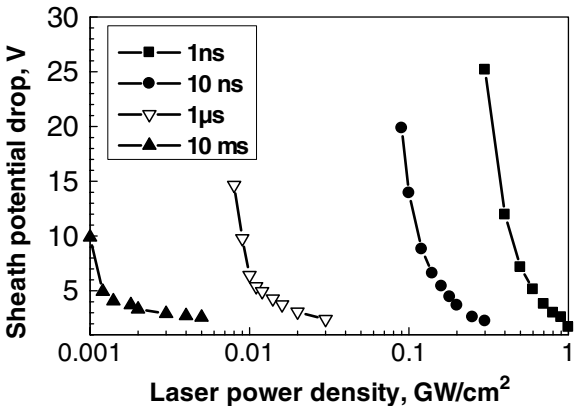

Figure 15. Potential drop in the sheath as a function of the laser power density [113].

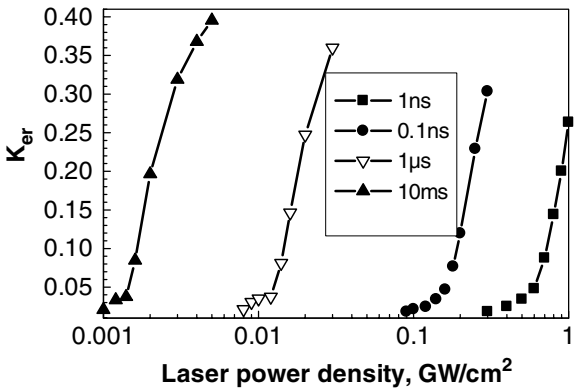

Figure 16. Fraction K_{er} dependence on the laser power density [113].

q_L—the plasma passes from weakly ionized ($\alpha \sim 0.01$) to fully ionized when T_e increased to a few electronvolts. In the fully ionized state, the plasma also contained doubly and triply charged ions.

The target temperature T_q was calculated considering only laser irradiation, i.e. neglecting the heat flux from the plasma by the ions and energy flux to the plasma by electron emission. The difference between T_0 and T_q (figure 17) calculated as a function on q_L was in the region of 300–3000 °C and demonstrated the plasma energy contribution in the target heat regime (K_e is the coefficient of laser power absorption in the electron beam relaxation zone). A large contribution of the plasma energy flux in the target energy balance was obtained, showing that the laser generated plasma significantly converts the absorbed laser energy to kinetic and potential energy of the plasma particles, which transport part of the energy through the electrostatic sheath to the solid surface. The calculated dependences of the target ablation rate per pulse versus full pulse energy density demonstrated agree well with measurements [116, 117].

12. Summary

The above review shows that Langmuir's pre-1930 scientific results significantly influenced and determined investigation of plasma–condensed matter interactions. Particularly important

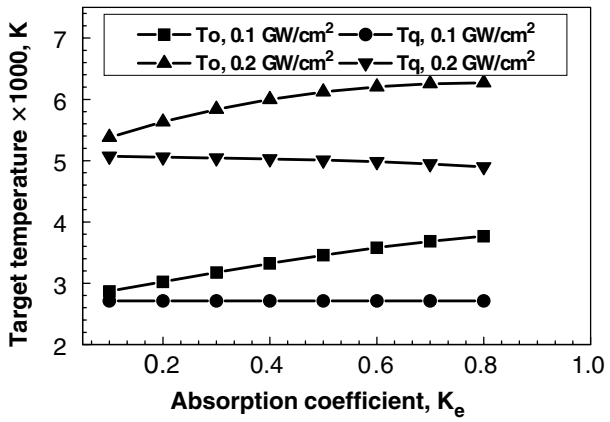

Figure 17. Target surface temperature T_0 calculated taking into account the plasma energy flux and target temperature T_q calculated without plasma energy inflow as a function for the coefficient of energy absorption K_e in the electron beam relaxation region with laser power q_L as a parameter [113].

were Langmuir's contribution to (i) material vaporization phenomena, including the relation between the surface temperature, saturated vapor pressure and rate of evaporation, (ii) electron emission from metals, (iii) space charge limited current, (iv) the probe method to determine the electron temperature and density in an ionized gas, (v) sheath formation at the boundary of an ionized gas with a wall, (vi) current flux-field characteristics in discharges and (vii) definition of the quasi-neutral 'plasma'.

In the present review, Langmuir's results were applied to investigate phenomena wherein the concentrated plasma interacts with condensed material, specifically in the cathode and anode spots in vacuum arcs and in plasma generation on the surface of a target irradiated by a pulsed laser. Vaporization at the target surface was described using a kinetic model calculating the net vapor flux as a difference between the direct Langmuir flux and the particle back flux determined by the particle collisions in the Knudsen layer. The evaporated mass flow should be impeded (i.e. have a lower velocity than the sound velocity) for the spot to ignite and operate. The important parameters are the electric field at the cathode surface in the spot and potential drop in the electrical sheath that determine the electron emission current from the cathode and heat fluxes carried by accelerated charge particles to the electrodes and to the adjacent plasma. The cathode potential drop is calculated by considering both the atom and electron evaporation and taking into account the plasma quasi-neutrality in the electron beam relaxation zone.

The relation between the vapor flux and the emitted electron flux depends on thermophysical material properties and for intermediate properties both fluxes are comparable, while the electron emission flux for tungsten and the vapor flux for volatile materials are too high. It was found that the Langmuir–Mackeown model determines this electric field for intermediate cathode materials and the space charge limited model can be used to describe the discharges with refractory electrodes. The hypothesis of the non-zero electric field at the sheath–plasma boundary provides the ratio of electron to ion currents observed in low current density, refractory cathode spots. A double sheath with a plasma cathode provides the current in the cathode region and the observed relatively low potential drop in the vacuum arc with volatile cathodes. Thus the sheath structure in essence provides current continuity in the cathode region for cathode materials with different thermophysical properties.

The mechanism of electron field emission in the vacuum arc cathode spot proposed by Langmuir can be applied to the relatively high current density cathode spot. In this case the heat flux to the cathode surface due to accelerated ions in the sheath significantly heats the cathode body. The models developed for nano-spots on flat cathodes and for transient spots on cathode protrusions showed that while the tunneling field emission current could contribute, the main electron emission mechanisms were T-Sh and T-F caused by a very high cathode temperature.

Plasma heating by Joule energy dissipation in the expanding plasma is the main energy source supporting the vacuum arc anode spot mode when the distance between the electrodes is large. In large gap arcs with relatively large area of anode surface, the anode can also be a collector of current without spot mode. A positive anode potential drop in arcs with the anode spot occurs. In contrast, the short gap arc is supported by the plasma generated by ionization of atoms evaporated from the cathode and the anode. In short gap arcs, the anode potential drop is negative due to the large plasma density in the gap.

Finally, it is well known that the plasma generated at a target intensely irradiated by a laser beam shields the target and reduces the efficiency of the interaction [115]. On the other hand, it was shown above that the plasma contacts the target by a sheath with a relatively large potential drop caused by the high electron temperature in the laser heated plasma. A high current of ions flows to the target, and the ions are accelerated across the sheath, bringing their potential and kinetic energy to the target. Electrons emitted from the heated target are similarly accelerated across the sheath in the opposite direction and heat the plasma. Therefore the laser energy absorbed in the plasma is converted to particle energy flux in the space charge sheath near the target [113]. The last effect is very important for laser applications.

In conclusion, successful understanding of complex phenomena in vacuum arcs and in laser generated plasma became possible due to Langmuir's pioneering works on plasma, sheaths, evaporation and electron emission, and his contributions can be expected to form the basis for future theoretical developments during the 21st century.

Acknowledgments

This research was supported by a Grant #727/07 from the ISF founded by the Israel Academy of Sciences. The author would like to thank to Professor R L Boxman for reading the paper and useful comments.

References

[1] Child C D 1911 *Phys. Rev.* **32** 492
[2] Langmuir I 1913 *Phys. Rev.* **2** 450

[3] Langmuir I and Blodgett K 1923 *Phys. Rev.* **22** 347
[4] Langmuir I and Blodgett K 1924 *Phys. Rev.* **24** 49
[5] Langmuir I 1923 *Phys. Rev.* **21** 419
[6] Langmuir I 1923 *Gen. Electr. Rev.* **26** 731
[7] Mott-Smith H M and Langmuir I 1926 *Phys. Rev.* **28** 727
[8] Compton K D, Turner L A and McCurdy W H 1924 *Phys. Rev.* **24** 597
[9] Langmuir I 1928 *Proc. Natl Acad. Sci.* **14** 627
[10] Debye P and Huckel E 1923 *Phys. Z.* **24** 185
Debye P and Huckel E 1923 *Phys. Z.* **24** 305
[11] Langmuir I 1925 *Phys. Rev.* **26** 585
[12] Tonks L and Langmuir I 1929 *Phys. Rev.* **33** 195
[13] Langmuir I 1929*Phys. Rev.* **33** 954
[14] Tonks L and Langmuir I 1929 *Phys. Rev.* **34** 876
[15] Langmuir I 1913 *Phys. Rev.* **2** 329
[16] Langmuir I 1916 *Phys. Rev.* **8** 149
[17] Langmuir I 1914 *Phys. Rev.* **4** 377
[18] Knudsen M 1915 Die maximale verdampfungsgeschwindigkeit des quecksilbers *Ann. Phys. Chem* **47** 697
[19] Bhatnagar P L, Cross E P and Krook M 1954 *Phys. Rev.* **94** 511
[20] Anisimov S I, Imas Yu A, Romanov G S and Khodyko Yu V 1971 *Action of High-Power Radiation on Metals* (Springfield, VA: Nat. Tech. Inform. Serv.)
[21] Knake O and Stranski I N 1956 *Prog. Met. Phys.* **6** 181
[22] Beilis I I 2006 *IEEE Trans. Plasma Sci* . **34** 855
[23] Anisimov S I 1968 *JETP* **37** 182
[24] Mott-Smith H M 1951 *Phys. Rev.* **82** 885
[25] Fisher J 1976 *Phys. Fluids* **19** 1305
[26] Beilis I I 1982 *Sov. Phys.— Dokl.* **27** 150
[27] Beilis I I 1986 *High Temp.* **24** 319
[28] Beilis I I 1985 *IEEE Trans. Plasma Sci* . **PS-13** 288
[29] Keidar M, Boyd I D and Beilis I I 2001 *J. Phys. D: Appl. Phys.* **34** 1675
[30] Keidar M, Boyd I D and Beilis I I 2004 *J. Appl. Phys.* **96** 5420
[31] Bohm D 1949 *Characteristics of electrical discharges in magnetic fields* ed A Guthrie and R Wakerling (New York: McGraw-Hill) chapter 3
[32] Lam S H 1965 *Phys. Fluids* **8** 73
[33] Franklin R N and Ockendon J R 1970 *J. Plasma Phys.* **4** 371
[34] Valentini H-B 1988 *J. Phys. D: Appl. Phys.* **21** 311
[35] Riemann K-U 1991 *Phys. Fluids* **25** 3331
[36] Riemann K-U 1997 *Phys. Plasmas* **4** 4158
[37] Riemann K-U 1989 *J. Appl. Phys.* **65** 999
[38] Valentini H-B 1996 *Phys. Plasmas* **3** 1459
[39] Godyak V and Sternberg N 1990 *IEEE Trans. Plasma Sci.* **18** 159
[40] Benilov M S and Franklin R N 1999 *J. Plasma Phys.* **62** 541
[41] Franklin R N and Snell J 2000 *Phys. Plasmas* **7** 3077
[42] Benilov M S 2003 *IEEE Trans. Plasma Sci.* **31** 678
[43] Sternberg N and Godyak V 2003 *IEEE Trans. Plasma Sci.* **31** 665
[44] Franklin R N J 2003 *J. Phys. D: Appl. Phys.* **36** R309–20
[45] Chodura R 1982 *Phys. Fluids* **25** 1628
[46] Riemann K-U 1994 *Phys. Plasmas* **1** 552
[47] Beilis I I, Keidar and Goldsmith M S 1997 *Phys. Plasmas* **4** 3461
[48] Beilis I I and Keidar M 1998 *Phys. Plasmas* **5** 1545
[49] Keidar M and Beilis I I 2005 *IEEE Trans. Plasma Sci.* **33** 1481
[50] Mackeown S 1929 *Phys. Rev.* **34** 611
[51] Beilis I I 1995 Theoretical modeling of cathode spot phenomena *Handbook of Vacuum Arc Science and Technology* ed R L Boxman *et al* (Park Ridge, NJ: Noyes) pp 208–56
[52] Compton K 1923 *Phys. Rev.* **21** 266
[53] Langmuir I 1927 *Z. Phys.* **46** 271
[54] Murphy E L and Good R H 1956 *Phys. Rev.* **102** 1464
[55] Dolan and Dyke W P 1954 *Phys. Rev.* **95** 327
[56] Beilis I I 1974 *Sov. Phys.—Tech. Phys.* **19** 257
[57] Dyke W P, Trolan I K, Martin E E and Barbour J P 1953 *Phys. Rev.* **91** 1043
[58] Bugaev S P, Litvinov E, Mesyats A G and Proskurovsky D I 1975 *Usp. Fiz. Nauk* **116** 101
[59] Beilis I I, Baksht R B, Oreshkin V I, Russkikh A G, Chaikovskii S A, Labetskii A Yu, Ratakhin N A and Shishlov A V 2008 *Phys. Plasmas* **15** 013501
[60] Boxman R L, Martin P J and Sanders D M (ed) 1995 *Handbook of Vacuum Arc Science and Technology* ed R L Boxman *et al* (Park Ridge, NJ: Noyes)
[61] Davis W D and Miller H C 1969 *J. Appl. Phys.* **40** 2212
[62] Beilis I I, Boxman R L and Goldsmith S 2000 *Surf. Coat. Technol.* **133–134** 91
[63] Schein J, Anders A, Binder R, Krishnan M, Polk J E, Qi N and Ziemer J 2002 *Rev. Sci. Instrum.* **73** 925
[64] Keidar M, Schein J, Wilson K, Gerhan A, Tang B, Idzkowski L, Krishnan M and Beilis I I 2005 *Plasma Sources Sci. Technol.* **14** 661
[65] Beilis I I 2001 *IEEE Trans. Plasma Sci.* **29** 657
[66] Juttner B 2001 *J. Phys. D: Appl. Phys.* **34** R103
[67] Lee T H and Greenwood A 1961 *J. Appl. Phys.* **32** 916
[68] Ecker G 1971 *Z. Naturf.* **26a** 935
[69] Ecker G 1973 *Z. Naturf.* **28a** 417
[70] Beilis I I 1974 *Sov. Phys.—Tech. Phys*. **19** 251
[71] Beilis I I, Lyubimov G A and Rakhovski V I 1970 *Sov. Phys.—Dokl.* **15** 254
[72] Beilis I I, Lyubimov G A and Rakhovski V I 1972 *Sov. Phys.—Dokl.* **17** 225
[73] Beilis I I and Lyubimov G A 1975 *High Temp.* **26** 1224
[74] Ecker G 1976 *IEEE Trans. Plasma Sci.* **4** 218
[75] Beilis I I 2003 *Contrib. Plasma Phys.* **43** 224
[76] Beilis I I 1988 *Sov. Phys.—Dokl.* **33** 125
[77] Kesaev I G 1968 *Cathode Processes in Electric Arcs* (Moscow: Nauka) in Russian
[78] Dushman S 1962 *Scientific Foundation of Vacuum Technique* ed J M Lafferty (New York: Wiley) p 691
[79] Kimblin C 1973 *J. Appl. Phys.* **44** 3074
[80] Hantzsche E 1974 *Beitr. Plasmaphys.* **14** 8
[81] Beilis I I 1988 *High Temp.* **26** 1224
[82] Finkelnburg W and Maecker H 1956 Electrishe bogen und thermishes plasma *Handbuch der Physik* vol XXII pp 254–444
[83] Rakhovsky V I 1976 *IEEE Trans. Plasma Sci.* **4** 81
[84] Selicatova S M and Lukatskaya I A 1972 *Sov. Phys.—Tech. Phys.* **17** 1202
[85] Perskii N E, Sysun V I and Khromoy Yu D 1989 *High Temp.* **27** 832
[86] Beilis I I 2004 *Appl. Phys. Lett.* **84** 1269
[87] Beilis I I 1996 *IEEE Trans. Plasma Sci.* **24** 1259
[88] Anders A, Anders S, Juttner B, Botticher W, Luck H and Schroder G 1992 *IEEE Trans. Plasma Sci.* **20** 466
[89] Juttner B 1995 *J. Phys. D: Appl. Phys.* **28** 516
[90] Juttner B 1997 *J. Phys. D: Appl. Phys.* **30** 221
[91] Juttner B 1999 *IEEE Trans. Plasma Sci* . **27** 836
[92] Jüttner B and Kleberg I 2000 *J. Phys. D: Appl. Phys.* **33** 2025
[93] Mesyats G A 2000 *Cathode Phenomena in Vacuum Discharge* (Moscow: Nauka)
[94] Beilis I I 2001 *IEEE Trans. Plasma Sci.* Part 2 **29** 844
[95] Rich J A 1961 *J. Appl. Phys.* **32** 1023
[96] Beilis I I, Lyubimov G A and Zektser M P 1988 *Sov. Phys.—Tech. Phys.* **33** 1132
[97] Krinberg I A and Paperny V 2002 *J. Phys. D: Appl. Phys.* **35** 549
[98] Beilis I I 2004 *Appl. Phys. Lett.* **85** 2739

[99] Beilis I I 1996 State of the theory of cathode spot phenomena *Vacuum Arc, 12th ISDEIV (Berkeley, CA, July 21–26, 1996)* pp 188–193
[100] Beilis I I 2007 *IEEE Trans. Plasma Sci.* **35** 966 Part 2
[101] Kimblin C W 1969 *J. Appl. Phys.* **40** 1744
[102] Miller H C 1995 Anode phenomena *Handbook of Vacuum Arc Science and Technology* ed R L Boxman *et al* (Park Ridge, NJ: Noyes) pp 308–64
[103] Ecker G 1961 Electrode components of the arc discharge *Ergeb. Der Exakten Naturw.* **33** 1–104
[104] Beilis I I 2000 *IEEE Trans. Compon. Packag. Technol.* **23** 334
[105] Germer L H and Haworth L H 1949 *J. Appl. Phys.* **20** 1085
[106] Kisluk P 1954 *J. Appl. Phys.* **25** 897
[107] Boyle W S and Germer L H 1955 *J. Appl. Phys.* **26** 571
[108] Beilis I I 2008 *Appl. Phys. Lett* . **92** 121501
[109] Tanberg R 1930 *Phys. Rev.* **35** 1080
[110] Kimblin C W 1974 *IEEE Trans. Plasma Sci.* **2** 310
[111] Beilis I I 2002 *IEEE Trans. Plasma Sci.* **30** 2124
[112] Hoffmann D H H, Blazevic A P, Rosmej Ni O, Roth M, Tahir N A, Tauschwitz A, Udrea S, Varentsov D, Weyrich K and Maron Y 2005 *Laser Part. Beams* **23** 47
[113] Beilis I I 2007 *Laser Part. Beams* **25** 53
[114] Gamaly E G, Rodea A V and Luther-Davies B 1999 *J. Appl. Phys.* **85** 4213
[115] Bogaerts A, Chen Z, Gijbels R and Vertes A 2003 *Spectrochim. Acta.* B **58** 1867
[116] Caridi F, Torrisi L, Margarone D, Picciotto M, Mezzasalma A A and Gammino S 2006 *Czech. J. Phys.* **56** B449
[117] Beilis I I 2008 *Radiat. Effects Defects Solids* **163** 317